Ab initio molecular-dynamics study of diffusion and defects in solid Li_3N

J. Sarnthein and K. Schwarz
Institut für Technische Elektrochemie, Technische Universität Wien, A-1060 Wien, Austria

P. E. Blöchl
IBM Research Division, Zurich Research Laboratory, CH-8803 Rüschlikon, Switzerland

(Received 30 October 1995)

We investigate defects and diffusion in solid Li_3N, a superionic conductor, using the projector-augmented-wave implementation of Car-Parrinello molecular dynamics. Static calculations are used to discuss the structure and formation of Li vacancies, where we also consider hydrogen interstitials. The barrier for lithium jumps to vacant adjacent sites in the Li_2N plane ($\perp c$) was found to be extremely small, namely, 0.004 eV, whereas jumps perpendicular to the Li_2N plane ($\| c$) have a barrier of 0.58 eV. Therefore diffusion in the plane ($\perp c$) is limited by the formation of vacancies, whereas the barrier dominates perpendicular ($\| c$) to the plane. A molecular-dynamics run at 800 K confirms the anisotropy of diffusion and leads to diffusion coefficients consistent with experiment. From the trajectories we deduce a microscopic diffusion mechanism and find that mainly isolated jumps take place.

I. INTRODUCTION

Lithium nitride is a superionic conductor with a high Li conductivity that has been studied intensively because of its potential utility as electrolyte in solid-state batteries.[1] In addition, the occurrence of ionic mobilities within a crystalline solid comparable to those of molten salts is of considerable fundamental interest. Experimentally the defect structure, phonon structure, and diffusion have been examined using x-ray,[2–4] Compton,[5] neutron,[6] and Raman scattering,[7] NMR,[8–11] and conductivity[12–14] measurements. Theoretically, the electronic structure has been studied with the linearized augmented plane wave (LAPW) method[15] and pseudopotentials[16] using density functional theory (DFT) as well as Hartree-Fock calculations.[17] It has been shown in these calculations and in Refs. 4 and 5 that the bonding is mainly ionic (near Li^+ and N^{3-}) but contains small covalent contributions and distortions of the highly polarizable N^{3-} ions. From the electronic charge distribution, the electric field gradient was derived on a first-principles basis[18] and was found to be in excellent agreement with experiment. These calculations have demonstrated that DFT calculations describe such systems well.

At about the same time, in a completely different approach, the dynamics in Li_3N has been studied by molecular-dynamics (MD) simulation.[19–21] The peculiarities of the dynamics are related to the hexagonal crystal structure. It consists of consecutive Li_2N planes [with the Li(2) positions] sandwiched by Li(1) atoms located between adjacent N atoms (Fig. 1). The MD simulations took into account only ionic interactions between atoms having a parametrized rigid ion potential. Nevertheless, they have been able to demonstrate the importance of the defect structure in the Li(2) sublattice and to reproduce the anisotropy of the mobility parallel and perpendicular to the *c* axis, thus confirming the picture deduced from experiments.[13]

However, before a thorough understanding of the conduction in Li_3N can be achieved, some open questions remain to be answered. Several experiments[3,10,13] have established that the charge carriers responsible for conduction are $V(2)$ vacancies, which consist of a vacant Li(2) site in the Li_2N plane. The barriers for jumps between vacancy sites are crucial for a microscopic-scale understanding of the diffusion process, which may take place simply as fast diffusion of isolated ions or in solitary events of correlated ion movements. To elucidate the latter point, a simulation of the Li_3N crystal at higher temperatures may provide new insight into the microscopic mechanism involved.

In this paper we report an application of *ab initio* MD calculations to the Li diffusion in Li_3N. We used the Car-

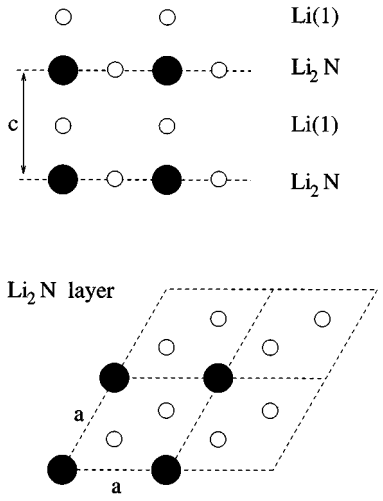

FIG. 1. The crystal structure of Li_3N consists of a layered hexagonal structure in which each N (filled circle) is surrounded by a hexagon of Li(2) (open circle) forming the Li_2N planes. Li(1) is sandwiched between such layers and lies on top of the N atoms at the center between two adjacent Li_2N layers. Our supercell contains two Li_2N layers [with eight Li(2) and four N atoms] and two Li(1) layers [with four Li(2) each].

Parrinello method[22] as implemented in the projector-augmented-wave (PAW) method recently developed by Blöchl.[23] After preliminary tests (Sec. III), we first performed static calculations with which we investigate the ionic and electronic structure of defects (Sec. IV A) and determined the barrier height for jumps of single Li^+ to a neighboring vacancy site (Sec. IV B). The Li^+ diffusion in the Li_2N plane faces only a negligible barrier and must therefore be limited by the number of available $V(2)$ defects, whereas perpendicular to the plane ($\|c$) the Li^+ must overcome a barrier of 0.58 eV. Second we investigated dynamical properties and simulated diffusion of a vacancy in solid Li_3N from first principles. We will show in Sec. V A how conductivity and diffusion of Li ions take place in the Li_2N plane ($\perp c$) and perpendicular to it ($\|c$).

II. EVIDENCE OF THE VACANCY MECHANISM OF DIFFUSION

In order to be able to relate our simulations to macroscopic measurements, we consider the dc ionic conductivity σ and the self-diffusion coefficient D^{Li} of Li ions, both of which follow an Arrhenius law,

$$\sigma \propto D^{\mathrm{Li}} \propto \exp\left(-\frac{\Delta H}{k_B T}\right), \tag{1}$$

where ΔH denotes the activation enthalpy of the process. The conductivity σ is described by the Nernst-Einstein equation

$$\sigma = n_\sigma D^\sigma \frac{Q^2}{k_B T}, \tag{2}$$

where the diffusing species are characterized by their charge Q and the diffusion coefficient D^σ, which also has an exponential temperature dependence. Charged $V(2)$ vacancies seem to be the predominant charge carriers in Li_3N.[13] The macroscopic density of charge carriers n_σ in Eq. (2) can be related to the formation energy E^f of the $V(2)$ vacancy by

$$n_\sigma = n \exp\left(-\frac{E^f}{k_B T}\right), \tag{3}$$

where n is the appropriate site concentration.

Bechthold *et al.*[10] gave the following evidence that Li ions diffuse mainly via a vacancy-assisted mechanism. They measured the Li ion diffusion coefficient D^{Li} in NMR experiments and related it to D^σ, which has been deduced[13] from conductivity measurements [Eq. (2)], where the macroscopic density of charged $V(2)$ vacancies $n_\sigma \approx 10^{25}$ m^{-3} has been estimated from the hydrogen impurity content of the sample. The two diffusion coefficients are related to each other by

$$n f D^{\mathrm{Li}} = n_\sigma f_\sigma D^\sigma, \tag{4}$$

where n stands for the density of Li ion sites per unit volume (6.72×10^{25} m^{-3}). In their analysis Bechthold *et al.*[10] assumed that the ratio of the correlation factors f_σ/f is close to 1 and independent of temperature. From the agreement of the activation enthalpy ΔH between conductivity (σ) and NMR (D^{Li}) measurements, they concluded that both methods probe the same transport mechanism. Therefore Li^+ ions seem to diffuse in a mechanism that involves negatively charged $V(2)$ vacancies.

III. METHODS AND TESTS

A. The PAW method

Our calculations are based on the *ab initio* MD method of Car and Parrinello[22] in the new implementation of the PAW method, which has been published in detail elsewhere.[23] The nuclear motion was treated classically and was combined with the electronic degrees of freedom within one formalism in which the equations of motion for electrons and nuclei were solved by means of MD. To describe the electronic structure we used DFT within the local density approximation (LDA) for exchange and correlation.[24] Valence electrons were expanded in a projector augmented plane wave basis set.

B. Computational details

If not stated otherwise, the calculations on Li_3N were performed in a hexagonal $2\times2\times2$ supercell of 32 atoms shown in Fig. 1, which was repeated periodically in space. The lattice parameters ($a=3.641$ Å, $c=3.872$ Å) of Li_3N were taken from x-ray experiments.[4] The electronic structure was determined using four high-symmetry k points. In the case of nominally charged simulation cells, a compensating uniform background was used in the calculation. This works well within a series of calculations where the charge remains constant. However, problems arise if one wants to compare the total energies of differently charged simulation cells because here it is difficult to define the Fermi energy common to all cells.

In a first test we varied the lattice parameter c in a unit cell containing one formula unit using eight special k points. The theoretical equilibrium at $c/a=1.051$ differed from the experimental $c/a=1.063$ by only about 1%. In addition we used the diatomic molecules Li_2 and N_2 as test cases for PAW. We achieved good convergence for the ground-state electronic properties with a plane-wave cutoff of 25 Ry and a cutoff for the electronic charge density of 50 Ry. The results agree well with other LDA calculations and are reported in Ref. 23 together with tests on various other systems.

In the dynamical simulations, the fictitious electron mass was chosen to be 1000 a.u., which allowed a time step of 10 a.u. (0.24 fs). We used a Nosé-Hoover thermostat[25] to keep the average ionic temperature at a fixed value and a second thermostat to correct for the energy transfer from the ionic to the electronic degrees of freedom.[26]

C. Electronic properties of ideal Li_3N

The band structure of Li_3N obtained with the very accurate full potential (FP) LAPW method[27] served as a test for PAW. Figure 2 shows the band structure obtained from FP LAPW, when nine k points in the irreducible wedge of the first Brillouin zone (IBZ) were used in the self-consistent field cycle. This is equivalent to a supercell of $2\times2\times2$ formula units with three independent high-symmetry k points as used in PAW. The energy levels of FP LAPW and PAW

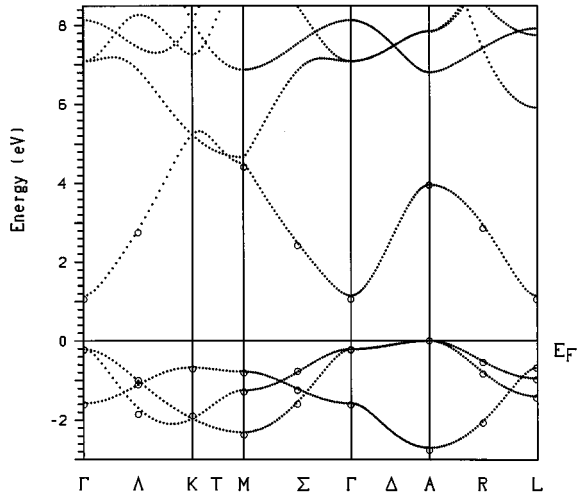

FIG. 2. Band structure of Li_3N calculated with FP LAPW (dots) and PAW (circles) using an identical Brillouin-zone sampling to obtain self-consistency.

agreed to within 0.07 eV. The band gap in this system (PAW 1.07 eV; FP LAPW 1.09 eV) was close to the fully converged FP LAPW gap of 1.13 eV when 70 instead of nine k points in the IBZ were used. These values significantly underestimate the experimental band gap of 2.2 eV, as can be expected from an LDA calculation. Also the cohesive energies (PAW -13.46 eV; FP LAPW -13.10 eV) agree to within 3%. Part of these small deviations may result from the use of different exchange correlation potentials (Refs. 24 and 28) in PAW and FP LAPW.

D. Electronic properties of lithium metal

To test the Li projectors used in our PAW scheme further we have also calculated the electronic structure of lithium metal in a supercell of 16 atoms in the bcc lattice using all eight high-symmetry k points. This corresponds to a calculation of a cell comprising two atoms and six independent k points. To describe the metallic structure, fractional occupations were used for some of the electronic states and optimized to find the minimum total energy. The PAW results agree well with data from the literature obtained with the FP LAPW (Ref. 29) or the augmented spherical wave (ASW) method[30] (Table I).

IV. STATIC CALCULATIONS

A. Structure and formation of $V(2)$ vacancies

It has been established by conductivity measurements[13] that charge carriers in Li_3N are predominantly defects of the

TABLE I. Lithium metal, supercell cell of 16 atoms in the bcc lattice with eight high-symmetry k points.

	PAW	FP LAPW[a]	ASW[b]
Cohesive energy (eV)	-1.80	-1.70	
Lattice constant (a.u.)	3.41	3.37	3.39
Bulk module (kbar)	146		140

[a]Reference 29.
[b]Reference 30.

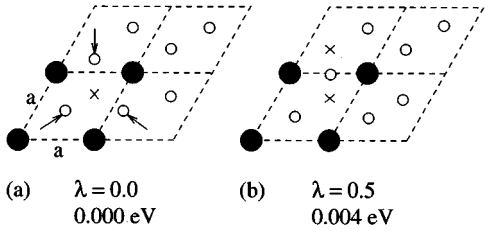

FIG. 3. Static $V(2)$ configurations associated with the Li(2) diffusion in the Li_2N plane ($\perp c$). Filled and open circles depict N and Li ions, respectively, whereas $V(2)$ vacancies are marked with a cross. The arrows indicate how the neighboring Li ions relax towards the vacancy. The reaction coordinate λ describes the relative coordinate of the Li ion that fills the $V(2)$ vacancy. (a) The relaxed $V(2)$ configuration with $\lambda=0.0$. (b) The symmetric split-vacancy configuration with $\lambda=0.5$ and a total energy of only $E_{\perp}^{S}=0.004$ eV higher than that in (a).

$V(2)$ type (a Li vacancy in the Li_2N plane). We have created this vacancy by removing one Li^+ ion from our $[Li_{24}N_8]$ supercell indicated by the cross in Fig. 3(a). During relaxation of the resulting $[Li_{23}N_8]^-$ supercell at $T=0$ K the three neighboring Li ions move towards this $V(2)$ site (as illustrated by the arrows) to compensate for the missing positive charge. The $V(2)$ vacancy must be charged, because the highest occupied bands in Li_3N are formed almost entirely of N $2p$ orbitals that are little affected by the absence of a Li^+ ion. If one generated an uncharged $V(2)$ defect by removing a neutral Li^0 atom, a hole in the valence band would appear and lead to a N^{2-} ion, an energetically very unfavorable process. Therefore, in the following the notation $V(2)$ will refer to the negatively charged state of the vacancy and only in some cases will the negative charge be stated explicitly.

To create the $V(2)$ vacancy, two mechanisms are discussed in the literature.

(a) The intrinsic generation of a vacancy interstitial in the solid-state reaction

$$2[Li_3N]^0 \rightarrow [Li_2N]^- + [Li_4N]^+,$$

$$\text{ideal crystal} \rightarrow [V(2)]^- + [I(1)]^+ \qquad (5)$$

involves a negatively charged $V(2)$ vacancy in the Li_2N plane and a positive interstitial in the Li(1) layer.

(b) $V(2)$ may be generated by substituting Li with hydrogen, so that a NH^{2-} can form, which has been seen experimentally.[13] This negative ion favors an additional Li^+ for its stabilization so that a Li^+ must be removed from a neighboring cell, leading to a $[V(2)]^-$ vacancy. This reaction scheme can be sketched

$$[Li_3N]^0 + [Li_2NH]^0 \rightarrow [Li_2N]^- + [Li_3NH]^+,$$

$$[V(2)H]^0 \rightarrow [V(2)]^- + [H]^+. \qquad (6)$$

This mechanism is supported by the observation that the conduction in Li_3N increases drastically with the hydrogen content of the samples.[13]

The charge density of the entities involved in Eq. (6) can be seen in Fig. 4. For the $V(2)$ vacancy a relaxation of the

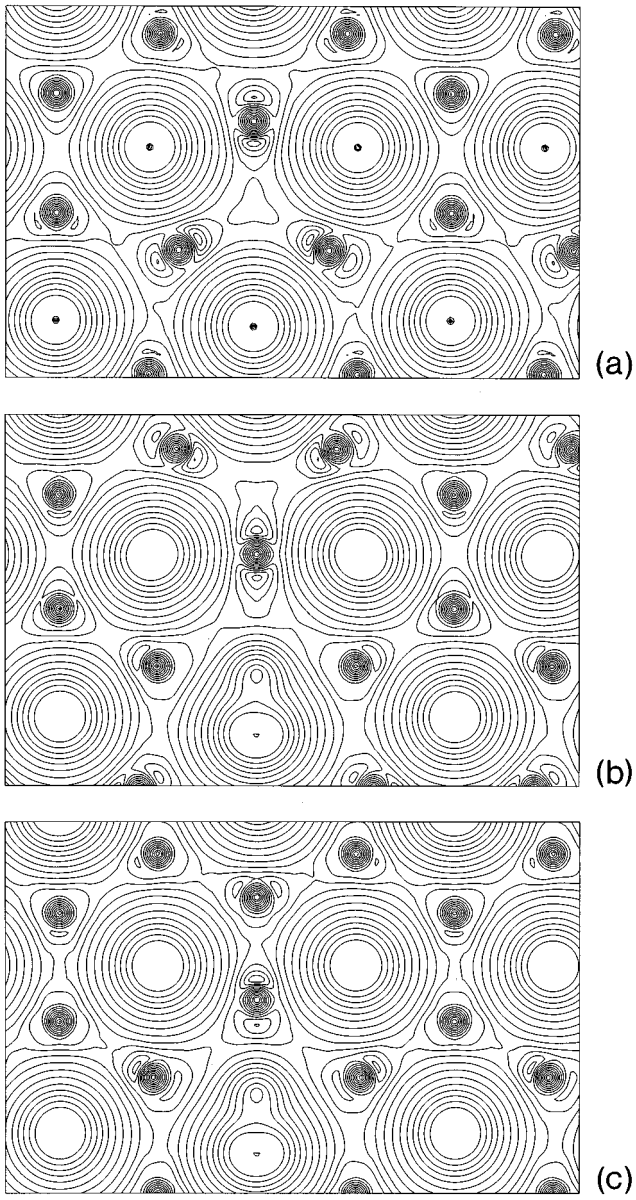

FIG. 4. Valence charge density corresponding to the nitrogen $2p$ bands in the Li_2N plane. The small circular peak contours represent the core region of the Li $2s$ charge densities. In a window similar to that in Fig. 3 we show the three defects that enter into Eq. (6): (a), (top) Li(2) vacancy $[V(2)]^-$; (b), (center) $[Li_2NH]^0$: one Li(2) substituted by H; (c), (bottom) H interstitial $[Li_3NH]^+$. Contour lines are spaced logarithmically.

three neighboring Li ions [illustrated in Fig. 3(a)] can clearly be seen from the density plot [Fig. 4(a)]. Between these three Li^+ ions there is only a small variation in density, which most likely originates from the highly polarizable N^{3-} ion. This situation leads to a rather flat potential around $V(2)$.

We started to investigate the neutral $[Li_2NH]^0$ case [Fig. 4(b)] by simply substituting one of the Li(2) with a hydrogen atom. During the substantial relaxation, the H atom moved away from the original Li(2) site and bonded to N with a distance of 1.06 Å, forming an NH^{2-} ion surrounded by five Li(2) ions within the Li_2N plane. Additionally, this N was displaced from its regular site by 0.22 Å. The formation of the NH^{2-} ion created a split-vacancy configuration similar to that in Fig. 3(b).

When a Li(2) ion was added to the supercell $[Li_2NH]^0$ to generate the configuration $[Li_3NH]^+$ [Fig. 4(c)], only minor changes occurred with respect to the NH^{2-} ion: It still has almost the same N-H distance (1.05 Å) and position as in $[Li_2NH]^0$, although it is surrounded by six Li(2) ions on nearly ideal sites in $[Li_3NH]^+$.

In both mechanisms [Eqs. (6) and (5)] of generating $V(2)$ vacancies, simulation cells of positive and negative charge appear. This makes it difficult to calculate the $V(2)$ formation energy E^f, which is defined by the corresponding total energy difference. This difficulty arises because, in our small supercells, a common Fermi energy is not well defined (as mentioned in Sec. III A).

B. Barriers E^m to move a vacancy

The conductivity σ due to diffusion of $V(2)$ vacancies depends exponentially on temperature via both n_σ and D^σ according to

$$\sigma \propto n_\sigma D^\sigma \propto \exp\left(-\frac{E^f+E^m}{k_B T}\right), \tag{7}$$

where E^f is associated with the formation of vacancies and E^m describes the barrier for a Li ion to hop to an adjacent vacancy site.

In order to determine E^m theoretically we have introduced a reaction coordinate λ, which is the projection of the Li position onto the line connecting the Li(2) sites occupied before and after the jump, respectively. We have constrained one Li ion to a certain value of λ with respect to the lattice (represented by the neighboring two N ions) and then relaxed all other ion positions in our $[Li_{23}N_8]^-$ supercell. Repeating this procedure for several values of λ allowed us to find the saddle point configuration for the respective jump.

1. Jumps in the Li_2N plane

In the Li_2N plane ($\perp c$) Fig. 3(a) corresponds to the ground state and $\lambda=0$. If we move the Li in the upper left subcell that is marked with an arrow towards the vacancy (cross) in the lower left subcell, we end up with the vacancy in the former cell ($\lambda=1$). Halfway on this path ($\lambda=0.5$) we pass through a transition state [Fig. 3(b)], which we term a split-vacancy configuration; i.e., two Li(2) sites are vacant (crosses). We relaxed the system for five values of λ and found a smooth potential curve as a function of the Li position. An analysis shows that Li(2) ions are situated in a very shallow potential in the Li_2N plane. The $V(2)$ ground-state configuration was only $E^m_\perp=0.004$ eV lower in energy than the relaxed split-vacancy configuration, so almost no barrier exists for these jumps. This is consistent with the experimental result of Wahl and Holland,[1,14] who determined the dielectric loss in Li_3N as a function of temperature. They found the Li ions to be in a very flat harmonic potential by fitting the relaxation rate with an energy barrier of 0.04 eV. In view of the smallness of this value, the agreement between theory and experiment is satisfactory. A point charge model yields the opposite ordering, and its energy for the

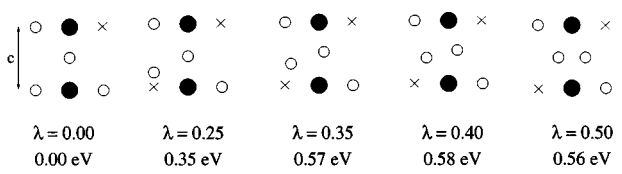

FIG. 5. Schematic path of Li ions moving perpendicular to the Li_2N plane ($\|c$) to fill a $V(2)$ vacancy (cross). Filled and open circles depict N and Li ions, respectively. The reaction coordinate λ describes the relative z coordinate of the Li ion that moves from the lower to the upper Li_2N plane. Shown are five distinct configurations for different λ and the respective total energy difference $E_{\|}^{S}$ with respect to the relaxed $V(2)$ configuration. The barrier is symmetric. Note that $E_{\|}^{S}$ for $\lambda=0.5$ is lower than for $\lambda=0.4$.

split-vacancy state is 0.08 eV *lower* than that of the $V(2)$ configuration. This means that the small magnitude of $E_{\perp}^{m}$ can already be understood for purely electrostatic interactions, but the difference between PAW and the electrostatic model indicates the importance of covalent effects in the bonding of Li_3N. This missing covalency may have caused the difficulties in the simulation of Wolf, Walker, and Catlow,[19] who succeeded in describing the general diffusion mechanism with its anisotropy but overestimated the diffusion constants by three orders of magnitude. Those authors used a pairwise ion potential and did not explicitly include covalency effects.

Based on our value for $E_{\perp}^{m}$ we argue that the experimental value of $\Delta H=E^{f}+E_{\perp}^{m}\approx 0.3$ eV (Refs. 8, 10, 12, and 13) for superionic conduction $\sigma_{\perp}$ originates mainly from E^{f}. Therefore the conduction in the Li_2N plane is mainly limited by the number of available charge carriers, namely, $V(2)$ vacancies. This is in contrast to the traditional model where a barrier of 0.2 eV is assumed in the diffusion mechanism.[3]

2. Jumps between Li_2N planes

For the vacancy diffusion perpendicular to the Li_2N plane ($\|c$) we have investigated three possible reaction paths and found a sizable barrier for all of them. The reaction coordinate λ describes the z coordinate of one Li ion in units of c. In Fig. 5 the initial situation ($\lambda=0$) is characterized by a $V(2)$ vacancy in the upper layer (cross). The three paths are as follows.

(i) The left Li(2) from the lower layer moves towards the vacancy. Halfway on this reaction path ($\lambda=0.5$) a dumbbell configuration is formed, where two Li ions are close to the Li(1) position. This barrier configuration is centrosymmetric with an activation energy of $E_{\|}^{m}=0.58$ eV, exhibiting a shallow local minimum of 0.56 eV at $\lambda=0.5$.

(ii) If the right Li(2) ion in the lower plane in Fig. 5 should move nearly $\|c$ to fill the $V(2)$ vacancy above (cross), it faces a barrier of 0.68 eV.

(iii) The obvious mechanism by which a Li(1) ion fills the neighboring $V(2)$ vacancy is associated with a rather high barrier of 1.2 eV.

Path (i) is the most likely reaction path for Li jumps $\|c$. In contrast to the case of jumps within the plane, the barrier ($E_{\|}^{m}=0.58$ eV) dominates $\Delta H=E^{f}+E_{\|}^{m}$. This explains the pronounced anisotropy of conduction in terms of barriers.

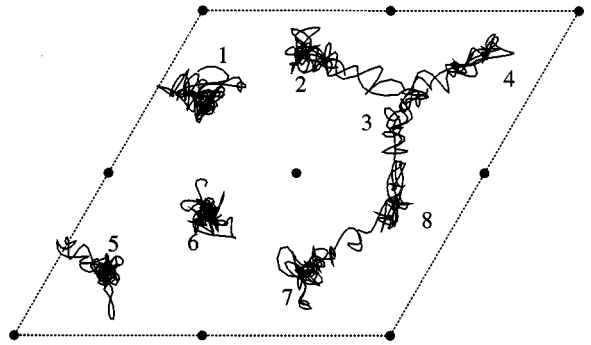

FIG. 6. Trajectories of Li(2) ions illustrating a typical diffusive event of the rattle-and-jump mechanism of diffusion in the Li_2N plane ($\perp c$). The nitrogen atoms remain very close to their equilibrium positions (filled circles). For a detailed description see text (Sec. V A).

V. DYNAMIC SIMULATIONS

A. Diffusion of a vacancy

In order to understand superionic conductivity, which takes place in a vacancy-assisted mechanism, we can simulate the diffusion of an isolated charged Li vacancy in Li_3N. For our PAW MD simulation we created a $V(2)$ vacancy by removing one Li^{+} ion from one Li_2N layer in our standard cell, leading to a $[Li_{23}N_8]^{-}$ supercell. We chose a temperature of 800 K (well below the melting point of 1086 K) and expanded the $T=0$ K value of the lattice constant a by 2% to describe the system at 800 K according to x-ray results.[2] We have equilibrated the system for a few picoseconds and then simulated it by PAW MD for about 6 ps.

1. Details of trajectories

To illustrate the predominant diffusion mechanism, the trajectories of Li ions in the Li_2N plane are shown in Fig. 6. The Li positions 1, 2, 3, 8, 7, and 6 are arranged in the form of a hexagon around the N atom at the center of the 2×2 cell. We only show a fraction of our simulation time, which, however, contains all the characteristics of the diffusion events. At the beginning of the depicted time slab from 3.5 to 5.0 ps, the vacancy was at site 7. From 3.5 to 4.0 ps, ions move simultaneously from site 3 to 8 and from 8 to 7. From 4.0 to 4.5 ps, sites 3 and 8 are in a split-vacancy configuration with an unsuccessful jump attempt of ion 2 towards site 3. From 4.5 to 5.0 ps, the ion on site 4 approaches site 3 but returns immediately. The Li ions at the sites 5, 6, and 1 are not involved in this diffusive event and rattle around their equilibrium positions. We chose this time slab to show the main features of the diffusion in the plane. They can be summarized as follows: (i) the importance of the vacancy, (ii) a large probability of the Li atoms to remain near their equilibrium positions, (iii) isolated jump attempts to a vacant neighboring site, and (iv) the stability of the nitrogen sublattice.

For motion of Li ions between Li_2N planes ($\|c$) we analyze the trajectories and extract the number of Li ions in the four planes of our supercell as a function of simulation time (Fig. 7). We see that at 2.1 ps a Li ion jumps from the filled

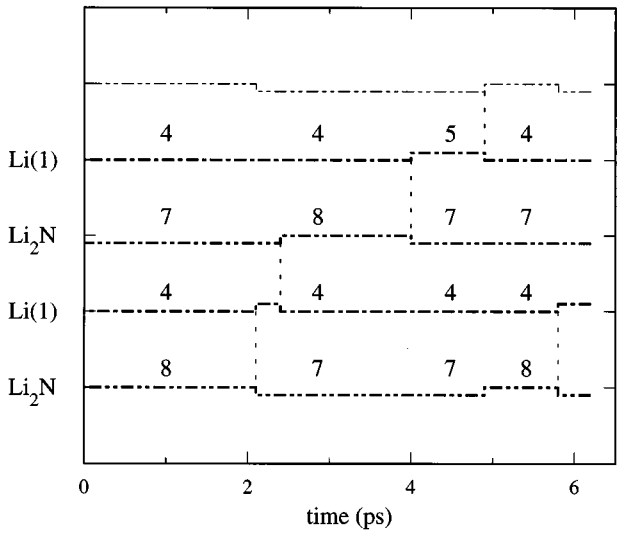

FIG. 7. Diffusion perpendicular to the Li_2N plane ($\|c$). Shown is the number of Li atoms that occupy each of the four planes in our supercell. The vacancy is initially in the upper Li_2N layer (occupation 7 instead of 8). The thin line on top is the periodic image of the lowest Li_2N layer. The dashed vertical lines mark an interplanar jump of a Li ion.

bottom Li(2) layer to the Li(1) layer forming an $I(1)$ interstitial (dumbbell configuration). Within about 0.5 ps one of the Li(1) in the dumbbell fills the vacancy in the top Li(2) layer. Now the vacancy is in the bottom layer and remains there until about 4.8 ps. At 4 ps a Li(2) from the upper Li_2N plane jumps to the top Li(1) layer, creating a second $V(2)$. At 4.8 ps there is another jump $\|c$ filling the $V(2)$ in the bottom layer (or the periodic image at the very top). A detail of this process is illustrated in Fig. 8 for the two crucial Li ions, where at the beginning of the depicted time window one of them (dashed line) is at a Li(1) site and the other (solid line) is in a Li(2) site in the lower Li_2N plane. The two Li ions share the Li(1) position from 4.4 to 4.8 ps before one of them (dashed line) fills a $V(2)$ vacancy in the upper Li_2N layer. The observation that both Li ions remain in the

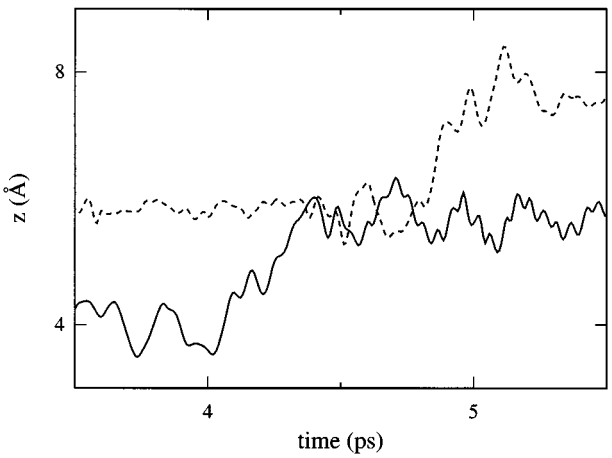

FIG. 8. Detail of the diffusion mechanism perpendicular to the Li_2N plane ($\|c$). Trajectories of the two Li ions involved in the process projected onto the c axis.

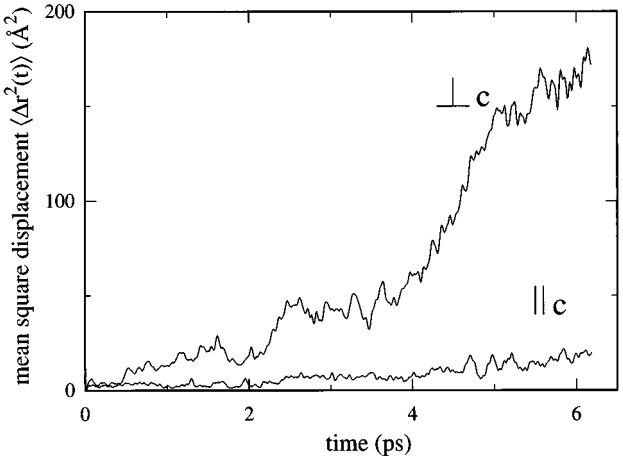

FIG. 9. Mean-square displacement $\langle \Delta r^2(t) \rangle$ of the vacancy in Li_3N. The mobility is high in the Li_2N plane ($\perp c$) (upper curve) and much smaller perpendicular to the Li_2N plane ($\|c$) (lower curve).

dumbbell configuration for about 0.4 ps is consistent with the associated local energy minimum of this configuration as discussed above (Sec. IV B, Fig. 5).

It should be mentioned that the rapid motion of Li ions between Li_2N planes ($\|c$) in our MD run differs from the more gradual movement reported by Wolf, Walker, and Catlow.[19]

2. Diffusion coefficient

In our simulation we monitored the mean-square displacement of Li ions $\langle \Delta r^2(t) \rangle$ for about 6 ps. The curves in Fig. 9 show that the self-diffusion in the Li_2N plane ($\perp c$) is much larger than that perpendicular to the Li_2N plane ($\|c$), a clear anisotropy in agreement with experiment. From the slope of the curves the diffusion coefficient D^σ of the diffusing species can be deduced using

$$\langle \Delta r_\| ^2(t) \rangle = 2D_\|^\sigma t + B_\| ,$$

$$\langle \Delta r_\perp ^2(t) \rangle = 4D_\perp^\sigma t + B_\perp , \tag{8}$$

where $B_\|$ and $B_\perp$ are the Debye-Waller factors parallel and perpendicular to the c axis, respectively.

According to the analysis presented in the previous paragraph (Figs. 7 and 8) our supercell contains two $V(2)$ vacancies during the time interval from 4.0 to 4.8 ps. Therefore the diffusion $\perp c$ was doubled during this period because twice as many $V(2)$ vacancies contribute to it. This observation explains the steep slope in the mean-square displacement

TABLE II. Diffusion coefficient of the $V(2)$ vacancy at 800 K. The vacancy concentration in the experimental samples was assumed to be equal to the hydrogen impurity content for this comparison.

	$D_\perp$ (10^{-8} m^2/s)	$D_\|$ (10^{-8} m^2/s)	$D_\perp / D_\|$
Theory	3.4	1.3	2.6
σ (Ref. 13)	35	24	1.5
NMR (Ref. 10)	73	39	3

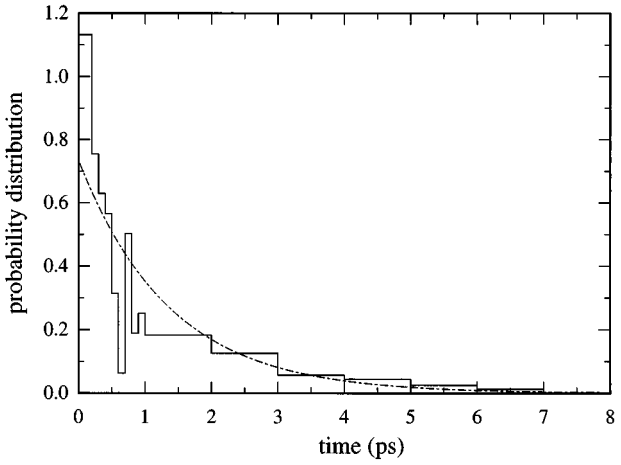

FIG. 10. Distribution of residence times τ_r between jumps in our simulation. The dash-dotted exponential curve is approached for totally uncorrelated single atom jump events.

$\langle \Delta r_\perp^2(t) \rangle$ in the respective time interval in Fig. 9. Table II refers to the diffusion of a single $V(2)$ between 0 and 4 ps, where we have also neglected the possibility of backward jumps.

The importance of the charge-carrier concentration n_σ at the chosen temperature makes a comparison with experiment difficult. Commonly, n_σ is estimated by the hydrogen impurity concentration 7.2×10^{25} m^{-3} in the experimental sample.[13] The assumed n_σ values are likely to be too small,[3] overestimating the experimental values of D^σ in Table II. Furthermore, the comparison may be hampered by the assumption that conductivity results taken around room temperature[13] can reliably be extrapolated to the temperature of our simulation ($T=800$ K).

3. Random jumps or correlated motion?

From an analysis of the trajectories of each ion we can learn about the microscopic time scales involved in diffusion. For this purpose we defined a sphere around each Li site in the crystal having a radius of 1/3 of the intersite distance. The average residence time of a Li atom in these spheres is $\langle \tau_r \rangle = 1.3$ ps. In view of the much smaller average flight time between spheres $\langle \tau_f \rangle = 0.2$ ps, an analysis in terms of single jumps appears to be valid.[31] This is to say that even at 800 K we do not observe a liquidlike diffusion mechanism in Li_3N, where these times would be of comparable magnitude.

To investigate the possibility of solitary events of the correlated motion of several ions, we show the distribution of residence times τ_r in Fig. 10. This histogram describes the probability $\dot{P}(\tau_r)$ of a Li ion leaving a site after a residence time τ_r. There are two cases.

(i) For random jumps the distribution should approach the dash-dotted exponential curve

$$\dot{P}(\tau_r) = \frac{1}{\langle \tau_r \rangle} \exp\left(-\frac{\tau_r}{\langle \tau_r \rangle} \right). \tag{9}$$

(ii) $\dot{P}(\tau_r)$ should peak above the exponential distribution expected for random events at small τ_r if a correlated motion of several ions (within one optical phonon period) occurs frequently. For example, we have observed a few events of up to four jumps occurring within 0.1 ps.

The portion of the histogram that lies above the exponential at small τ_r indicates that less than 10% of the jumps occur in a concerted way. Therefore, we do not find strong evidence of correlated motions, although this would be favored by the small supercell of our MD simulation.

TABLE III. Vibrations of ions around their equilibrium positions described by the Debye-Waller factor B (in Å^2). The MD simulations were performed in a supercell containing no vacancy. The experimental data have been refined in a harmonic model (Ref. 3).

	Li(2) $\parallel c$	Li(2) $\perp c$	Li(1) $\parallel c$	Li(1) $\perp c$	N $\parallel c$
300 K theory	0.04	0.02	0.01	0.03	0.01
300 K expt.	0.03	0.01	0.01	0.02	0.01
800 K theory	0.10	0.07	0.02	0.09	0.02
800 K expt.	0.07	0.04	0.03	0.04	0.03

B. Debye-Waller factors

From our MD run we can also estimate Debye-Waller factors in Li_3N. We will show below that they have an anisotropy as in experiment but opposite to the one expected from the calculated diffusion mechanism.

We simulated the motion of the ions at 300 and 800 K in a supercell without a vacancy. The mean-square displacement $\langle \Delta r_\alpha^2(t) \rangle$ of species α equals the Debye-Waller factor B_α as long as no diffusion takes place [Eq. (8)]. In Table III we compare our results to data from x-ray experiments that have been refined in a harmonic model.[3] Our simulation reproduces well the experimental results for vibrations in the planes of the crystal ($\perp c$). The vibrations of N ions are negligible both in experiment and in our simulation, which might be related to the eightfold coordination of each N ion. Owing to the cell geometry the vibration $\parallel c$ of Li(1) and N occurs with identical amplitudes. These values are smaller in the simulation than in experiment, because we have only simulated the phonons related to N ions $\parallel c$ at the k point A, whereas the phonons at Γ were suppressed by the small size of the supercell.

A related detail has been reported by Wolf, Walker, and Catlow[19] in their conventional MD simulation. They found a "rumpling" of the Li(2) atoms in the Li_2N plane, which leads to a double peak in the probability density function of Li ions along the c axis. We, however, found a smooth Gaussian-like shape for this as well as for all other distributions that led to the $\langle \Delta r_\alpha^2(t) \rangle$.

The relatively small vibrations of Li(2) $\perp c$ support the observation that Li(2) ions remain close to their sites if they are not involved in a specific jump (Fig. 6). Li ions should therefore diffuse primarily in single jumps, in agreement with our analysis in Sec. V A 3.

It is interesting to note that the preferred direction of diffusion is perpendicular to the direction of the largest amplitude of vibrations, the latter lying in the c direction ($\parallel c$) for Li(2) and perpendicular ($\perp c$) for Li(1) as shown in Table III.

The obvious mechanism of diffusion $\perp c$ in the much more open Li(1) plane does not occur, although it would be supported by the large amplitude of vibration of Li(1) $\perp c$ (Table III). In this context it is useful to remember that the Li(1)-N distance is shorter than the Li(2)-N distance,[1] indicating a stronger bond of the former.

VI. CONCLUSIONS

In this work we have demonstrated that *ab initio* molecular-dynamics calculations with the PAW method can provide new insight into various aspects of diffusion in solids. First, the electronic structure of the charge-carrying defects in Li_3N has been calculated considering the relaxed lattice. Then, atomistic insight into the diffusion mechanism has been gained by studying well-defined transition states along the reaction paths corresponding to jumps of Li ions between sites. For instance, by comparing activation energies we have learned that for Li diffusion in the plane, not the individual jumps but the creation of the $V(2)$ defects is the rate-limiting quantity for diffusion. Finally, we were able to describe statistical aspects of the general mechanisms of diffusion with a dynamical simulation. In our molecular-dynamics simulation we have shown that a description of diffusion in terms of individual uncorrelated jumps is still valid at 800 K, and we have obtained theoretical diffusion coefficients at this temperature that agree well with experimental data.

ACKNOWLEDGMENTS

This work was supported by the Austrian Science Foundation (FWF Project No. P9213) and the IBM joint research Project No. 80601511 and has benefited from the collaboration within the Human Capital Mobility Network on ''Ab initio (from electronic structure) calculation of complex processes in materials (Contract No. ERBCHRXCT930369).'' One of us (J.S.) thanks Roberto Car for stimulating discussions.

[1] A. Rabenau, *Advances in Solid State Physics* (Vieweg, Braunschweig, 1978), Vol. 18, p. 77; Solid State Ionics **6**, 277 (1982).
[2] H. Schulz and K. H. Thiemann, Acta Crystallogr. Sec. A **35**, 309 (1979).
[3] U. Zucker and H. Schulz, Acta Crystallogr. Sec. A **38**, 568 (1982).
[4] H. Schulz and K. Schwarz, Acta Crystallogr. Sec. A **34**, 999 (1978).
[5] P. Pattison, N. K. Hansen, and J. R. Schneider, Acta Crystallogr. Sec. A **40**, 38 (1984).
[6] W. Kress, H. Grimm, W. Press, and J. Lefebvre, Phys. Rev. B **22**, 4620 (1980).
[7] H. R. Chandrasekar, G. Bhattacharya, R. Mignoni, and H. Bilz, Phys. Rev. B **17**, 884 (1978).
[8] R. Messer, H. Birli, and K. Differt, J. Phys. C **14**, 2731 (1981)
[9] D. Brinkmann, M. Mali, J. Roos, R. Messer, and H. Birli, Phys. Rev. B **26**, 4810 (1982).
[10] E. Bechthold-Schweikert, M. Mali, J. Roos, and D. Brinkmann, Phys. Rev. B **30**, 2891 (1984).
[11] M. Mali, J. Roos, and D. Brinkmann, Phys. Rev. B **36**, 3888 (1987).
[12] U. v. Alpen, A. Rabenau, and G. H. Talat, Appl. Phys. Lett. **30**, 621 (1977).
[13] J. Wahl, Solid State Commun. **29**, 485 (1979).
[14] J. Wahl and U. Holland, Solid State Commun. **27**, 237 (1978).
[15] P. Blaha, J. Redinger, and K. Schwarz, Z. Phys. B **57**, 273 (1984).
[16] G. Kerker, Phys. Rev. B **23**, 6312 (1978).
[17] R. Dovesi, C. Pisani, F. Ricca, C. Roetti, and V. R. Saunders, Phys. Rev. B **30**, 972 (1984).
[18] P. Blaha, K. Schwarz, and P. Herzig, Phys. Rev. Lett. **54**, 1192 (1985).
[19] M. L. Wolf, J. R. Walker, and C. R. A. Catlow, J. Phys. C **17**, 6623 (1984).
[20] M. L. Wolf, J. Phys. C **17**, L285 (1984).
[21] S. Ihara and K. Suzuki, Phys. Lett. A **110**, 265 (1985).
[22] R. Car and M. Parrinello, Phys. Rev. Lett. **55**, 2471 (1985).
[23] P. E. Blöchl, Phys. Rev. B **50**, 17 953 (1994).
[24] J. P. Perdew and A. Zunger, Phys. Rev. B **23**, 5048 (1981); D. Ceperley and B. J. Alder, Phys. Rev. Lett. **45**, 566 (1980).
[25] S. Nosé, Mol. Phys. **52**, 255 (1984); W. G. Hoover, Phys. Rev. A **31**, 1965 (1985); S. Nosé, Prog. Theor. Phys. Suppl. **103**, 1 (1991).
[26] P. E. Blöchl and M. Parrinello, Phys. Rev. B **45**, 9413 (1992).
[27] P. Blaha, K. Schwarz, and R. Augustyn, WIEN95, Technische Universität Wien, 1995. [Improved and updated Unix version of the original copyrighted WIEN-code, which was published by P. Blaha, K. Schwarz, P. Sorantin, and S. B. Trickey, Comput. Phys. Commun. **59**, 399 (1990)].
[28] L. Hedin and B. I. Lundquist, J. Phys. C **4**, 2064 (1971).
[29] J. Nobel, S. Trickey, P. Blaha, and K. Schwarz, Phys. Rev. B **45**, 5012 (1992).
[30] V. L. Moruzzi and C. B. Sommer, *Calculation of Electronic Properties of Ordered Alloys: A Handbook* (World Scientific, Singapore, 1995).
[31] M. J. Gillan, in *Ionic Solids at High Temperatures*, edited by A. M. Stoneham (World Scientific, Singapore, 1989).